The Journal of Neuroscience, December 1, 1998, *18*(23):9573–9584

Single-Cell RT-PCR and Functional Characterization of Ca^{2+} Channels in Motoneurons of the Rat Facial Nucleus

T. D. Plant, C. Schirra, E. Katz, O. D. Uchitel, and A. Konnerth

I. Physiologisches Institut, Universität des Saarlandes, 66421 Homburg, Germany

Voltage-dependent Ca^{2+} channels are a major pathway for Ca^{2+} entry in neurons. We have studied the electrophysiological, pharmacological, and molecular properties of voltage-gated Ca^{2+} channels in motoneurons of the rat facial nucleus in slices of the brainstem. Most facial motoneurons express both low voltage-activated (LVA) and high voltage-activated (HVA) Ca^{2+} channel currents. The HVA current is composed of a number of pharmacologically separable components, including 30% of N-type and ~5% of L-type. Despite the dominating role of P-type Ca^{2+} channels in transmitter release at facial motoneuron terminals described in previous studies, these channels were not present in the cell body. Remarkably, most of the HVA current was carried through a new type of Ca^{2+} channel that is resistant to toxin and dihydropyridine block but distinct from the R-type currents described in other neurons.

Using reverse transcription followed by PCR amplification (RT-PCR) with a powerful set of primers designed to amplify all HVA subtypes of the α_1-subunit, we identified a highly heterogeneous expression pattern of Ca^{2+} channel α_1-subunit mRNA in individual neurons consistent with the Ca^{2+} current components found in the cell bodies and axon terminals. We detected mRNA for α_{1A} in 86% of neurons, α_{1B} in 59%, α_{1C} in 18%, α_{1D} in 18%, and α_{1E} in 59%. Either α_{1A} or α_{1B} mRNAs (or both) were present in all neurons, together with various other α_1-subunit mRNAs. The most frequently occurring combination was α_{1A} with α_{1B} and α_{1E}. Taken together, these results demonstrate that the Ca^{2+} channel pattern found in facial motoneurons is highly distinct from that found in other brainstem motoneurons.

Key words: motoneuron; facial nucleus; calcium channel; calcium current; ω-conotoxin-GVIA; ω-agatoxin-IVA; ω-conotoxin-MVIIC; single-cell RT-PCR; α_1-subunit

Neuronal Ca^{2+} channels have been subdivided on the basis of their electrophysiological and pharmacological properties into low voltage-activated (LVA) or T-type channels (Huguenard, 1996) and high voltage-activated (HVA) channels, a class that includes L-, N-, P/Q-, and R-types (Hofmann et al., 1994; Dunlap et al., 1995; Wheeler et al., 1995). The HVA channel types are not easily distinguishable from their biophysical properties and have mainly been characterized by their different sensitivities to pharmacological modulators and inhibitory toxins. HVA channels are complexes composed of a pore-forming α_1-subunit together with modulatory β-, α_2/δ-, and, at least in skeletal muscle, γ-subunits (Hofmann et al., 1994; Catterall, 1995; Dunlap et al., 1995). To date, six HVA α_1-subunits have been identified: α_{1A}, α_{1B}, α_{1C}, α_{1D}, α_{1E}, and α_{1S}. Although it is clear that α_{1B} forms the N-type channel, α_{1C} and α_{1D} the L-type channel, and α_{1S} the skeletal muscle channel/voltage sensor, the subunit composition of the P/Q- and R-type channel is less clear. α_{1A} is thought to form the P/Q-type and α_{1E} the R-type. The α_1-subunits that compose the T-type channel α_{1G} and α_{1H} have recently been cloned (Perez-Reyes et al., 1998).

In motoneurons, Ca^{2+} channels are clearly involved in the release of transmitter from the axon at the neuromuscular junction (NMJ). In addition, they are also expressed in the soma and dendrites, where they have been shown to be involved in the control of firing properties, both directly and through the activation of other Ca^{2+}-dependent membrane conductances (Viana et al., 1993). Furthermore, Ca^{2+} signaling, possibly involving Ca^{2+} entry through voltage-gated Ca^{2+} channels, has been implicated as a mechanism involved in the degeneration of motoneurons in amyotrophic lateral sclerosis (ALS) (Uchitel et al., 1988; Llinás et al., 1993; Mosier et al., 1995). Changes in Ca^{2+} channel types involved in transmitter release at the endplate also accompany axon growth and muscle reinnervation after axotomy of adult motoneurons (Katz et al., 1996).

The Ca^{2+} channel types present at the nerve terminals of facial motoneurons have been extensively characterized (Uchitel et al., 1992; Protti and Uchitel, 1993; Katz et al., 1996, 1997). Although a number of studies describe the Ca^{2+} channel types present in motoneurons in other regions of the brainstem and in the spinal cord, both in brain slices and in culture (Mynlieff and Beam, 1992; Viana et al., 1993; Umemiya and Berger, 1994, 1995), those in the facial nucleus have not been studied in detail (Umemiya et al., 1993). This precludes the comparison of the Ca^{2+} channels present in the soma with those at nerve terminals and study of their possible differential distribution. We therefore characterized voltage-gated Ca^{2+} channels in the facial nucleus of the neonatal rat. The electrophysiological and pharmacological properties were studied using the patch-clamp technique in slices of

Received April 8, 1998; revised Aug. 25, 1998; accepted Sept. 9, 1998.

This study was supported by grants from the Bundesministerium für Bildung, Wissenschaft, Forschung und Technologie (Neurotraumatologie Programm) and the Universität des Saarlandes (ZFK-1997). We thank Dr. Félix Viana for his helpful comments on this manuscript and Erle Eilers, Heide Krempel, Nicole Rothgerber, and Reiko Trautmann for technical assistance.

Correspondence should be addressed to Dr. T. D. Plant at his present address: Institut für Pharmakologie, Freie Universität Berlin, 14195 Berlin, Germany.

Dr. Katz's present address: Departamento de Biología, Facultad de Ciencias Exactas y Naturales, Universidad de Buenos Aires, Ciudad Universitaria (1428), Buenos Aires, Argentina.

Dr. Uchitel's present address: Laboratorio de Fisiologia y Biología Molecular, Departamento de Ciencas Biologicas, Facultad de Ciencias Biologicas, Universidad de Buenos Aires, Ciudad Universitaria (1428), Buenos Aires, Argentina.

 0270-6474/98/189573-12$05.00/0

the brainstem. In addition, we also studied the expression of mRNA for the different α_1-subunits of the HVA Ca^{2+} channel in individual neurons using reverse transcription (RT) followed by PCR amplification of the resulting cDNA.

MATERIALS AND METHODS

Preparation. Neonatal Wistar rats [age: postnatal day 1 (P1)–P7] were decapitated, and the brainstem was removed rapidly and placed in ice-cold saline. Transverse slices (150-250 μm thick) were prepared using a vibrating slicer as described previously (Edwards et al., 1989). After they were cut, the slices were incubated at 37°C for ~1 hr and thereafter at 25°C until they were transferred to the recording chamber. For some control experiments, rat hippocampal and cerebellar slices were used.

The recording chamber containing the slice was placed on the stage of an upright microscope (Axioskop FS, Zeiss, Jena, Germany) and viewed using infrared differential interference contrast video microscopy (Stuart et al., 1993). In early experiments, the facial nucleus was localized by retrograde labeling with the carbocyanine fluorescent dye 1,1′-dioctadecyl-3,3,3′,3′-tetramethylindocarbocyanine perchlorate (DiI) (Molecular Probes, Eugene, OR). Briefly, rat pups were anesthetized by hypothermia, and a small incision was made behind one ear. The facial nerve was localized, and a suspension of dye [2.5 mg/ml, 20% ethanol, 80% saline with 0.1% bovine serum albumin (also see Mynlieff and Beam, 1992)] was injected into the nerve using a glass micropipette. The incision was sutured. Rats were killed 1-2 d after injection. Slices containing retrogradely labeled facial motoneurons were clearly visible when viewed using epifluorescence (see Fig. 1). In later experiments, unlabeled slices containing the facial nucleus were identified visually under a dissecting microscope using dark-field illumination and in the experimental set up using infrared differential interference contrast videomicroscopy.

Patch-clamp recording. Whole-cell currents were measured using the patch-clamp technique with an EPC 7 or EPC 9 patch-clamp amplifier and Pulse software (Heka, Lambrecht, Germany). Patch pipettes were made of borosilicate glass (Hilgenberg, Malsfeld, Germany) and coated with a silicone resin (GE-Silicones, Bergen op Zoom, The Netherlands). The electrodes had resistances of 2-3 MΩ when filled with the internal solution that contained (in mM): 130 CsCl, 20 TEACl, 1 EGTA, 4 MgATP, 0.4 GTP, and 10 HEPES (titrated to pH 7.2 with CsOH). Leakage correction was performed using a P/4 protocol at a potential of −100 mV. Series resistance compensation (≥70%) was used in all experiments.

Solutions and chemicals. The standard saline contained (in mM): 125 NaCl, 2.5 KCl, 2 $CaCl_2$, 1 $MgCl_2$, 1.25 NaH_2PO_4, 26 $NaHCO_3$, and 20 glucose (pH 7.3 when gassed with 95% O_2 and 5% CO_2). To record Ca^{2+} channel currents, this solution was exchanged for one containing (in mM): 105 NaCl, 20 TEACl, 2.5 KCl, 1 or 0.5 $BaCl_2$, 1 $MgCl_2$, 1.25 NaH_2PO_4, 26 $NaHCO_3$, 20 glucose, with 0.5 μM tetrodotoxin (TTX), 1 μM strychnine, and 10 μM bicuculline (pH 7.3 when gassed with 95% O_2 and 5% CO_2). In experiments in which peptide toxins were applied, the bath solution also contained 0.1 mg/ml cytochrome C. Because the addition of cytochrome C reduced the TTX block of Na^+ currents, the TTX concentration was raised to 1 μM. ω-Conotoxin (CTx)-GVIA was obtained from Sigma (Deisenhofen, Germany), ω-Conotoxin-MVIIC was from Alomone Labs (Jerusalem, Israel), different batches of ω-agatoxin (Aga)-IV were obtained from Peptide Institute (Osaka, Japan) or Pfizer Research, and ω-Aga-TK was from Alomone Labs. The toxins were prepared as stocks in water and kept frozen at −20°C. Toxins were applied either locally from a pipette located close to the cell, by bath perfusion, or by addition to the bath while the perfusion was stopped. No difference in blocking efficacy was observed with the different application methods. The experiments were all performed at room temperature (20-25°C).

Cellular RNA harvest and RT. The contents of individual neurons were harvested, and mRNA was transcribed into cDNA as described in detail previously (Lambolez et al., 1992; Plant et al., 1997). Thereafter, the tube was stored at −80°C until it was used for PCR amplification. Positive controls, using total RNA from rat brain, and negative controls, using water instead of RNA or without reverse transcriptase, were performed in parallel to the reactions for material isolated from single cells.

First PCR amplification of the rat brain isoforms of the α_1-subunit of the HVA Ca^{2+} channel. PCR amplification was performed using partially degenerate primers (see Fig. 3) that amplify fragments of all of the rat brain isoforms of the HVA calcium channel α_1-subunits, α_{1A}–α_{1S}. The primers were selected for regions of homology between segment S6 of repeat III and segment S5 of repeat IV (see Fig. 3). The sense and antisense primers used were: Calpha-up [5′-AT(C/T) (A/G)TC ACC TTC CAG GAG CA-3′] and Calpha-lo [5′-GCG TAG ATG AAG AA(A/G/C) AGC AT-3′]. The positions of the primers on the individual sequences in the GenBank are as follows: the Calpha-up (upstream or sense, 20-mer) primer positions (position 1 is the first base of the initiation codon) were 4384 on α_{1A} (P/Q-type: M64373, rat brain), 4252 on α_{1B} (N-type: M92905, rat brain), 3496/3505 on $\alpha_{1Ca/b}$ (L-type: M67516/M67515, rat brain), 3451 on α_{1D} (L-type: M57682, rat brain), 4123 on α_{1E} (R-type: L15453, rat brain), 1054 on α_{1S} (skeletal muscle-type; L04684, rat brain), and the Calpha-lo (downstream or antisense primer, 20-mer) primer positions were 4954 on α_{1A}, 4822 on α_{1B}, 4105/4114 on $\alpha_{1Ca/b}$, 4072 on α_{1D}, 4702 on α_{1E}, and 1687 on α_{1S}. The lo primer fully matched with α_{1B}, α_{1D}, α_{1E}, and α_{1S}-subunits, but had one mismatch with α_{1A} and two mismatches with α_{1C} (see Fig. 3). The sizes of the amplified fragments calculated from the published sequences were 590 bp for α_{1A} and α_{1B}, 599 bp for α_{1E}, 629 bp for α_{1C}, 641 bp for α_{1D}, and 653bp for α_{1S}. A mixture containing the fragments α_{1A}, α_{1B}, or α_{1E} should appear as a single DNA band on agarose gel electrophoresis. Mixtures of these subunits with α_{1C}, α_{1D}, or α_{1S} should give two separate bands.

The first PCR amplification was performed as described previously (Lambolez et al., 1992; Plant et al., 1997) except that 40 pmol of each primer was used. Before PCR, samples were heated to 94°C for 3 min. Each PCR cycle consisted of denaturation at 94°C for 30 sec, annealing at 55°C for 30 sec, and elongation at 72°C for 1 min. Forty cycles were performed with a programmable thermocycler (Biometra, Göttingen, Germany). After PCR, samples were heated to 72°C for 10 min. Ten microliters of the amplification reaction were run with a molecular weight marker (ϕX174, *Hae*III-digested) on a 1.5% agarose gel stained with ethidium bromide. The product of the first PCR was cut out of the agarose gel and used for a second amplification step.

Second PCR amplification for restriction analysis. To obtain a sufficient amount of α_1-subunit fragments for a restriction analysis, a second round of amplification was performed (Lambolez et al., 1992; Plant et al., 1997) using the up and lo primers described above. After the second PCR amplification in a final volume of 100 μl, under the same conditions as those described above, a chloroform–isoamylalcohol extraction and ethanol precipitation were performed. The DNA was then resuspended in 18 μl H_2O, and 3 μl aliquots were digested by one of the restriction enzymes (see Figs. 4, 5). Five enzymes were chosen, *Drd*I, *Bpm*I, *Hinc*II, *Afl*II, and *Acc*I (New England Biolabs, Schwalbach, Germany), which selectively cut the brain α_{1A}, α_{1B}, α_{1C}, α_{1D}, and α_{1E} isoform PCR fragments, respectively. The calculated lengths of the fragments generated by the restriction enzymes are shown in Figure 3. The skeletal muscle isoform α_{1S} contained a restriction site for *Hinc*II (at position 1527, yielding fragments of 474 and 179 bp) and three sites for *Bpm*I (at positions 1369, 1467, and 1536, giving fragments of 316, 170, 98, and 69 bp). Because of the large number of fragments with *Bpm*I, α_{1S} is easily distinguishable from α_{1B}. The identity of the α_{1S}-subunit can be confirmed by the presence of a single specific restriction site for *Cla*I (at position 1466), yielding fragments of 413 and 240 bp. To guarantee complete digestion, five units of each enzyme were used for an incubation time of 3 hr. The restriction reaction was then analyzed by electrophoresis on a 2% agarose gel as described above.

Optimization of PCR sensitivity. Using rat brain RNA (see below), PCR conditions were optimized so that a PCR product could be detected from 10 pg of total RNA (see Fig. 4*A*), without contamination caused by unspecific amplification. To test the efficiency of the PCR, cDNA was synthesized from 100 ng total RNA by RT (as described above). The cDNA was diluted to 0.01-10 ng/μl using sterile water and used as a template for the PCR. Total RNA from other tissues and specific brain regions were tested to check that tissue-specific product patterns were observed. Furthermore, single cells, known to express a cell-specific mRNA pattern, were also used to test the PCR amplification.

RNA preparation and amplification. Total RNA was prepared from fresh brain (P12 and adult), pancreas (P14–P17), kidney (adult), heart (adult), skeletal muscle (adult), and adrenal gland (adult) of the rat using the RNeasy Midi-Kit (Qiagen, Hilden, Germany). The total RNA was treated with DNase I to exclude genomic DNA contamination of the RNA preparation and possible amplification of genomic DNA. As additional controls, the RT reaction was performed in the absence of reverse transcriptase or RNA. The RT reactions and the amplification and

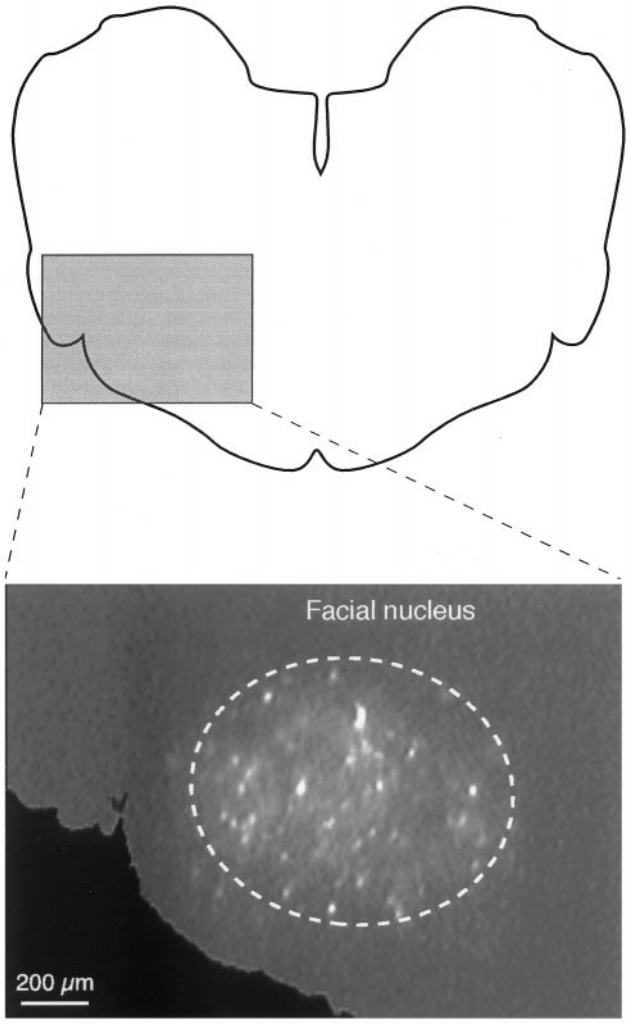

Figure 1. Localization of the facial nucleus by retrograde labeling. Scheme of a transverse brainstem slice obtained from video micrographs in transmitted light. The enlarged region in epifluorescence shows the facial nucleus stained with DiI injected into the facial nerve 2 d previously. To aid the localization of the nucleus, the edge of the slice measured in transmitted light (*dark area* at *left*) has been superimposed on the fluorescence image.

analysis steps were performed as described above, starting with 10 ng of total RNA.

Genomic DNA preparation and amplification. Genomic DNA was prepared from adult rat brain using the genomic DNA isolation kit (Boehringer Mannheim, Mannheim, Germany). PCR amplification was performed with 200 ng of rat genomic DNA.

RESULTS

Biophysical properties of Ca^{2+} channel currents

Experiments were performed in a total of 156 cells, identified in initial experiments by retrograde labeling (Fig. 1) and later by inspection of the slice by dark-field illumination followed by infrared differential interference contrast video microscopy. Large Ca^{2+} channel currents were activated by steps in membrane potential from a holding potential of −80 mV to potentials more positive than −70 mV in Ca^{2+}- and Ba^{2+}-containing solutions. In the majority of experiments, Ba^{2+} was chosen as charge carrier to decrease the contribution of K^+ currents incompletely blocked by internal Cs^+ and TEA^+ and external TEA^+. In addition, to improve the control of the membrane potential and decrease series resistance errors caused by large currents, most experiments were performed using 1 or 0.5 mM Ba^{2+} as the charge carrier. Under these conditions, potential steps from a holding potential of −80 mV revealed two major components of Ca^{2+} channel current in facial motoneurons (Fig. 2*A*). A fast transient component of current was activated during steps positive to −70 mV, and a more sustained, slowly inactivating component was activated at potentials more positive than −50 mV. These resemble the LVA (T) and HVA currents in other neuron types, respectively. In 5% of neurons, only HVA currents were observed. In neurons that expressed both LVA and HVA currents, there was no clear change in their relative proportions with age during the first postnatal week. A marked difference in the relative proportions of current should be reflected in the ratio of the current amplitude at −40 mV, where the current is mainly LVA (see below), to that at −10 mV, where the HVA current dominates. There was no significant difference (*t* test, 0.05 level) in the values obtained during the first postnatal week; all values were ~0.3 (0.309 ± 0.018, $n = 22$, at P1–P2, and 0.252 ± 0.027, $n = 5$, at P6–P7). A change in the holding potential from −80 to −60 mV completely abolished the LVA current component (Fig. 2*B*). The remaining current was exclusively HVA and inactivated only slowly and incompletely during 250 msec potential steps. A difference in the time course of the current at the two holding potentials is most clear near −50 mV (Fig. 2*A,B*). At potentials more positive than −10 mV, only the amplitude of current, not the time course, was affected by the change in holding potential. Currents at potentials of more than −10 mV, activated from a holding potential of −60 mV, were smaller, but when scaled-up they had time courses similar to those at the same membrane potential but activated from −80 mV. These results suggest that the fast transient component, most clearly seen at more negative potentials, was completely inactivated by the shift in holding potential, whereas the current activated by larger depolarizations was only partially inactivated. Furthermore, the LVA current contributes only a small fraction of the current at potentials positive to −10 mV.

The current–voltage (*I–V*) relations for the peak inward current at the two holding potentials are shown in Figure 2*C*. From the *I–V* relation it is clear that a component of current that activates above −70 mV is abolished by the change in holding potential, shifting the activation threshold close to −50 mV. The maximum inward current was between −10 and −20 mV at both holding potentials. During steps from a holding potential of −80 mV, the maximum inward current was 1537.2 ± 114.0 pA ($n = 45$) in 1 mM Ba^{2+} and 995.9 ± 64.4 ($n = 31$) in 0.5 mM Ba^{2+}.

The potential dependence of inactivation of both components of current was studied in more detail. Currents were measured during a test pulse to −10 mV, where the current is mainly HVA, preceded by 15 sec conditioning pulses to potentials between −100 and +10 mV. The resulting inactivation curve is shown in Figure 2*D* (●). Even after conditioning pulses of this length, inactivation was incomplete, and a noninactivating component remained. For the current inactivated by the 15 sec pulse, a fit of a Boltzmann distribution to the data gave a potential for half-inactivation of −45.5 ± 1.6 mV ($n = 7$), and a slope factor k of 13.3 ± 1.1. On average, the current that was not inactivated by a 15 sec pulse was 7.5% of the total current. The inactivation of the LVA component was studied using a test pulse to −40 mV preceded by a 500 msec conditioning pulse to potentials between −100 and −45 mV. Currents were reduced at conditioning potentials more positive than −85 mV, and little further reduction

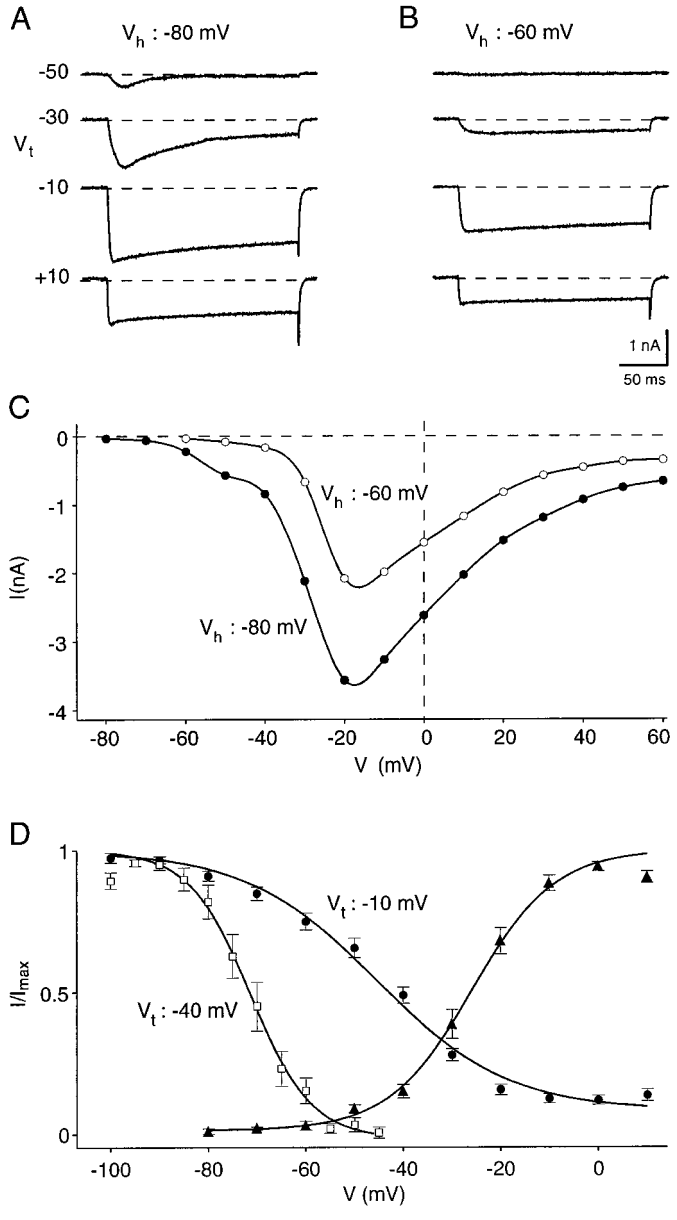

Figure 2. Biophysical properties of Ca^{2+} channel currents. Ca^{2+} channel currents measured during 250 msec steps to the potentials (V_t) indicated from holding potentials (V_h) of −80 mV (*A*) and −60 mV (*B*). *C*, *I–V* relations at −80 mV (●) and −60 mV (○) from the same motoneuron as *A* and *B*. *D*, Inactivation curves measured using a test pulse to −40 mV after a 500 msec conditioning pulse to potentials between −100 and −50 mV (□), and using a test pulse to −10 mV after a 15 sec conditioning depolarization to potentials between −100 and +10 mV (●). The points were fitted with a Boltzmann distribution: $I/I_{max} = \{(1 - N/(1 + \exp((V - V_{1/2})/k))\} + N$, where k is the slope parameter, $V_{1/2}$ is the potential at which the current was inactivated by 50%, and N is the noninactivating component of current. The respective values for $V_{1/2}$ and k were −71.3 mV and 6.25 at −40 mV and −45.4 mV and 13.5 at −10 mV. Also shown is the mean activation curve, measured from tail currents at the end of 250 msec pulses (▲). The fit parameters from the fitted Boltzmann distribution (as above) were −25.9 mV and −8.9 for $V_{1/2}$ and k, respectively.

of the current was observed at potentials positive to −55 mV. The inactivation curve for the transient component, after subtraction of the current that was not inactivated by a 500 msec pulse, is shown in Figure 2*D*. On average, 34 ± 2% ($n = 5$) of the current at −40 mV was resistant to inactivation and was probably HVA. The transient current was half-inactivated at a conditioning potential of −71.6 ± 2.0 mV; the slope factor k was 5.3 ± 0.2. These results suggest that most facial motoneurons express LVA (T) and HVA components, the T-type channel being completely inactivated at more positive holding potentials. Figure 2*D* also shows the mean activation curve estimated from tail currents at the end of 250 msec depolarizing impulses, where the current is mainly HVA. The midpoint of the activation curve is at a potential of −26 mV.

PCR analysis of Ca^{2+} channel α_1-subunits

Previous studies on Ca^{2+} channel α_1-subunit mRNA expression in single cells have used antisense RNA amplification (Bargas et al., 1994) or have amplified each subunit in separate reactions using nested PCR with specific outer and inner primers (Yan and Surmeier, 1996). In contrast, we designed partially degenerate primers to amplify all of the HVA α_1-subunits in the same reaction and then identified the individual subunits that were present by restriction analysis.

The region of the α_1-subunits of the Ca^{2+} channel that was amplified, the primers used, and the details of the restriction analysis are illustrated in Figure 3 and outlined in detail in Materials and Methods. Before using RT-PCR on material isolated from single motoneurons, we tested the ability of the primers to amplify fragments of all forms of the HVA Ca^{2+} channel α_1-subunits. For this, total RNA was isolated from tissues known to express different isoforms of the α_1-subunits. Using rat brain RNA (see below), PCR conditions were optimized so that a PCR product could be detected from 10 pg of total RNA. Figure 4*A* shows the result of an experiment in which different amounts of DNA were used in the PCR and shows that a product was still detected with 10 pg. No product was detected using genomic DNA as template or in reactions without reverse transcriptase (Fig. 4*B*).

The Ca^{2+} channel mRNA detected in adult whole brain after RT-PCR amplification and analysis of the amplified fragments using specific restriction enzymes is shown Figure 4*C*. In this RNA, α_{1A}, α_{1B}, and α_{1E} were clearly detected; α_{1C}, α_{1D}, and α_{1S} were not detected. The α_1-subunits detected are summarized in Table 1. The results are consistent with the very widespread expression of the α_{1A}, α_{1B}, and α_{1E} and the lower, spatially more restricted occurrence of α_{1C} and α_{1D} (Tanaka et al., 1995; Ludwig et al., 1997) being reflected in the concentrations of their mRNAs. As shown in Table 1, the pattern was different in RNA isolated from specific regions of the brain. In the adult neocortex and hippocampus, α_{1A}, α_{1B}, α_{1C}, α_{1D}, and α_{1E} were detected as also shown from *in situ* hybridization (Tanaka et al., 1995; Ludwig et al., 1997). In cerebellar RNA, α_{1A}, α_{1B}, and α_{1E} were detected at both P12 and in the adult; α_{1D} was detected only at P12. In the brainstem, only α_{1A}, α_{1B}, and α_{1E} were detected.

In total RNA from regions other than the brain, we detected tissue-specific expression patterns for the mRNAs (Table 1). Thus, in skeletal muscle a fragment was amplified that was cut by *Hinc*II into two fragments and by *Bpm*I into multiple fragments, consistent with the pattern expected for α_{1S} (see Materials and Methods), a result that was confirmed using *Cla*I. In the kidney, we detected mRNA for the α_{1A}- and α_{1D}-subunits. In the heart, α_{1A}, α_{1B}, α_{1C}, and α_{1D} were detected. In mRNA from the pancreas, the neuroendocrine form α_{1D} was clearly detected, together with α_{1A}, α_{1B}, and α_{1C}. In the adrenal gland, the pattern was α_{1A}, α_{1B}, and α_{1C}.

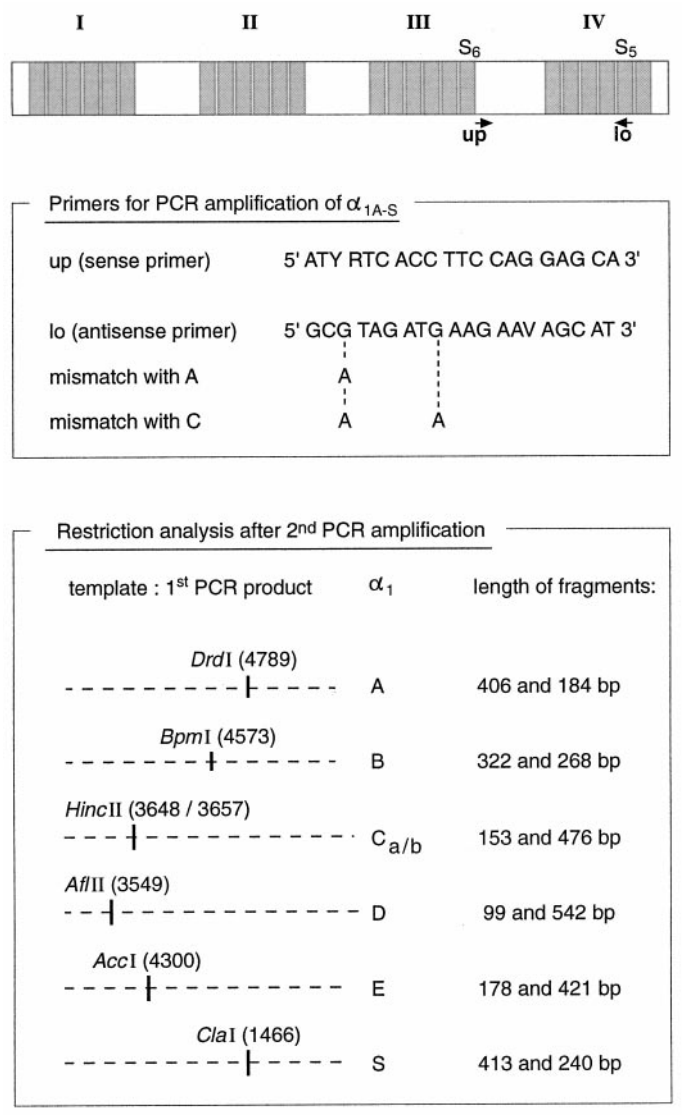

Figure 3. Molecular analysis of Ca^{2+} channel α_1-subunits in single neurons. *Top*, Positions of primers on the coding sequence for the α_1-subunits of the voltage-gated Ca^{2+} channel. The *shaded regions* indicate the locations of the putative transmembrane domains. *Middle*, Sequences of the *up* and *lo* primers indicating the positions of mismatches where appropriate. *Bottom*, Details of the restriction analysis for the detection of individual α_1-subunits after a second round of PCR amplification using the primers described for the first PCR amplification. The figure show the positions of the restriction sites and the lengths of the expected fragments.

Thus, from RNA in different brain regions and other tissues, the partially degenerate primers amplify DNA fragments that correspond in length to those predicted from the cDNAs of the HVA Ca^{2+} channel α_1-subunits. Furthermore, digestion with restriction enzymes specific for the individual subunits gave restriction fragments of the predicted sizes. We also detected region-specific patterns of α_1-subunit RNA expression similar to those expected from previous studies using RT-PCR or *in situ* hybridization. No amplification was observed using genomic DNA as the template for the PCR reaction. In none of the tissues or regions did we see a PCR product of unexpected length or restriction fragments of unexpected lengths that would suggest the amplification of an unknown subunit. Similarly, after parallel digestion with all restriction enzymes, no fragments were detected that were resistant to digestion, also ruling out unspecific amplification.

We then tested the ability of the RT-PCR method with the chosen primers to detect Ca^{2+} channel α_1-subunits in single neurons in which the cell's content was harvested through the patch pipette as described previously (Lambolez et al., 1992; Plant et al., 1997). As controls in single cells, we studied the subunit expression in cells known from *in situ* hybridization to have a characteristic subunit composition. The results of the first PCR reaction and the restriction analysis are shown in Figure 5, and the data from all cells that gave a positive result are summarized in Table 2. In four cerebellar Purkinje neurons, we detected only mRNA for α_{1A} (Fig. 5*A*, Table 2). In contrast, in granule cells of the dentate gyrus, which were chosen because the region expresses all brain HVA subunits at moderate to high levels (Tanaka et al., 1995; Ludwig et al., 1997), we detected a more heterogeneous pattern, with all subunits represented in the three cells but clear differences between individual cells. As expected from both electrophysiological measurements, which demonstrate a large component of L-type current (Eliot and Johnston, 1994), and *in situ* hybridization studies (Tanaka et al., 1995; Ludwig et al., 1997), α_{1C} or α_{1D} were present in all three cells. Figure 5*B* shows data from a cell in which α_{1C} and α_{1D} were detected.

In motoneurons of the facial nucleus, we detected mRNA for α_1-subunits after the first round of PCR amplification in 22 of 30 neurons. The agarose gels in Figure 5*C,D* show the product of the first PCR reaction and the results of the restriction digest after the second PCR for two cells in which different patterns of α_1-subunit expression were detected. For the neuron in Figure 5*C*, α_{1A}, α_{1B}, and α_{1E} were detected, whereas for that in Figure 5*D*, only α_{1A} and α_{1C} were detected. For all neurons studied, the heterogeneous pattern of α_1-subunit mRNA expression shown in Table 2 was obtained. The most frequently occurring messages were those for α_{1A}, α_{1B}, and α_{1E}, with α_{1C} and α_{1D} also observed in smaller proportion of cells. However, even those mRNAs that were most frequently observed were not detectable in all cells. Thus, α_{1A} was detected in 86% of neurons, α_{1B} in 59%, α_{1C} in 18%, α_{1D} in 18%, and α_{1E} in 59%. As is clear from Table 2, the pattern detected in individual cells was highly variable. However, mRNAs for either α_{1A} or α_{1B} were present in all neurons (Fig. 5*C,D*), with those for the other subunits showing a much higher variability. Of the two most dominant subunits, α_{1A} and α_{1B}, α_{1A} was present alone in 41% of neurons and α_{1B} was present alone in 14%. In the remaining 45% of neurons, both α_{1A} and α_{1B} were detected. Surprisingly, two neurons showed the restriction pattern with *Bpm*I and *Hinc*II expected for the skeletal muscle isoform of the α-subunit, α_{1S}, in combination with α_{1A}. The identity of the fragment thought to be from α_{1S} was confirmed by its cleavage into fragments of the expected length by *Cla*I. This subunit is not usually associated with or widely considered to be expressed in the brain, but a fragment has been cloned from rat brain cDNA (Chin et al., 1992). Similar patterns of α_1-subunit expression were detected independently of whether the nucleus was harvested together with the cytoplasm, suggesting that genomic DNA is not being amplified from single cells as is also shown above for total RNA. With the primers used, we have no evidence for a new subunit in single motoneurons. Simultaneous digestion of the PCR product with all of the restriction enzymes resulted in a complete disappearance of the parent band (data not shown).

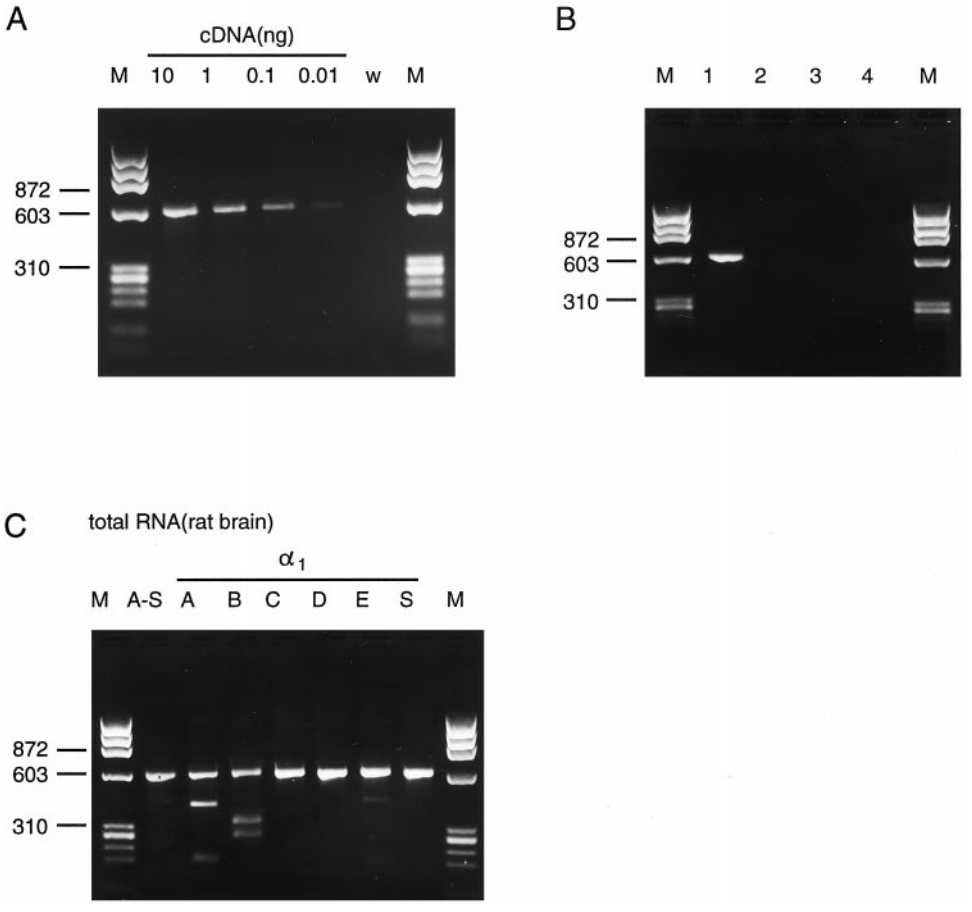

Figure 4. RT-PCR analysis of Ca^{2+} channel α_1-subunits. *A*, Ethidium bromide-stained gel (1.5%) showing the amplified fragments produced when 10, 1, 0.1, and 0.01 ng of input cDNA from whole-brain total RNA were used in the PCR. The lanes marked *M* and *W* are the molecular weight marker ϕX174/*Hae*II and the RT-PCR without RNA, respectively. *B*, Ethidium bromide-stained gel (1.5%) showing the absence of amplification of genomic DNA. *Lane 1*, RT-PCR with 10 ng of total RNA from rat brain. *Lane 2*, RT-PCR with 10 ng of total RNA from whole brain, but without reverse transcriptase. *Lane 3*, PCR with 200 ng of genomic DNA. *Lane 4*, RT-PCR without RNA. *M*, Molecular weight marker. *C*, Analysis of Ca^{2+} channel α_1-subunits in RNA from whole brain (adult). The lane marked *A-S* shows the band corresponding to the fragments obtained after the first PCR. Lanes marked *A, B, C, D, E*, and *S* show the fragments obtained after a second PCR reaction and restriction digest with the enzymes *Drd*I, *Bpm*I, *Hinc*II, *Afl*II, *Acc*I, and *Cla*I, respectively.

Table 1. RT-PCR analysis of calcium channel α_1-subunit RNA expression in total RNA from different tissues from the rat

		Subunit					
Tissue	Age	α_{1A}	α_{1B}	α_{1C}	α_{1D}	α_{1E}	α_{1S}
Brain	Adult	+	+	−	−	+	−
Neocortex	Adult	+	+	+	+	+	−
Hippocampus	P12	+	+	+	+	+	−
Cerebellum	P12	+	+	−	+	+	−
Cerebellum	Adult	+	+	−	−	+	−
Brainstem	Adult	+	+	−	−	+	−
Skeletal muscle	Adult	−	−	−	−	−	+
Kidney	Adult	+	−	−	+	−	−
Adrenal	Adult	+	+	−	+	−	−
Pancreas	P14–P17	+	+	+	+	−	−
Heart	Adult	+	+	+	+	−	−

Pharmacological profile of whole-cell Ca^{2+} channel currents

Effects of Ni^{2+} and Cd^{2+}

Ni^{2+} (50 μM) did not clearly differentiate between LVA and HVA currents. The current at −40 mV, after a 1 sec prepulse to −100 mV, was inhibited by 40 ± 1% (n = 6), whereas the current at −10 mV, after a 1 sec prepulse to −60 mV, was inhibited by 50 ± 3% (n = 6). At concentrations of 100 or 200 μM, Cd^{2+} blocked nearly all of the current at −10 mV. With 100 μM Cd^{2+}, the mean inhibition was 92.8 ± 0.5% (n = 4).

Pharmacological characterization of HVA current components

To characterize the HVA component of the Ca^{2+} current in these neurons with respect to different HVA channel types, which are difficult to differentiate from their voltage dependence and kinetics, we used various antagonists. Currents were measured during short depolarizing (10-50 msec) pulses from −80 to −10 mV, the minimum of the *I–V* relation, applied at 10 or 15 sec intervals.

Effect of ω-CTx-GVIA

The neurotoxin, ω-CTx-GVIA (Olivera et al., 1984), a specific antagonist of N-type Ca^{2+} channels (Mogul and Fox, 1991; Regan et al., 1991; Olivera et al., 1994), used at concentrations of 1 μM or more, had a clear effect in most cells, producing, at the holding potential used (Stocker et al., 1997), a rapid irreversible block of the Ca^{2+} channel current, when applied locally or to the bath solution (Fig. 6). The inhibition by ω-CTx-GVIA was 24 ± 3% (n = 5) at a concentration of 1 μM and 32 ± 4% (n = 5) at 10 μM, values that are not significantly different (t test, 0.05 level). Only one cell did not respond to ω-CTx-GVIA. It is notable that the time course of the current was largely unaffected by the toxin treatment (Fig. 6*A*).

Effect of dihydropyridines

Dihydropyridines (DHPs) are modulators of L-type Ca^{2+} channel currents in neurons. In facial motoneurons, nitrendipine, at the relatively high concentration of 10 μM, had only a very weak but reversible inhibitory effect on Ca^{2+} channel currents. The block that was small (Fig. 6*B*) and thus difficult to measure

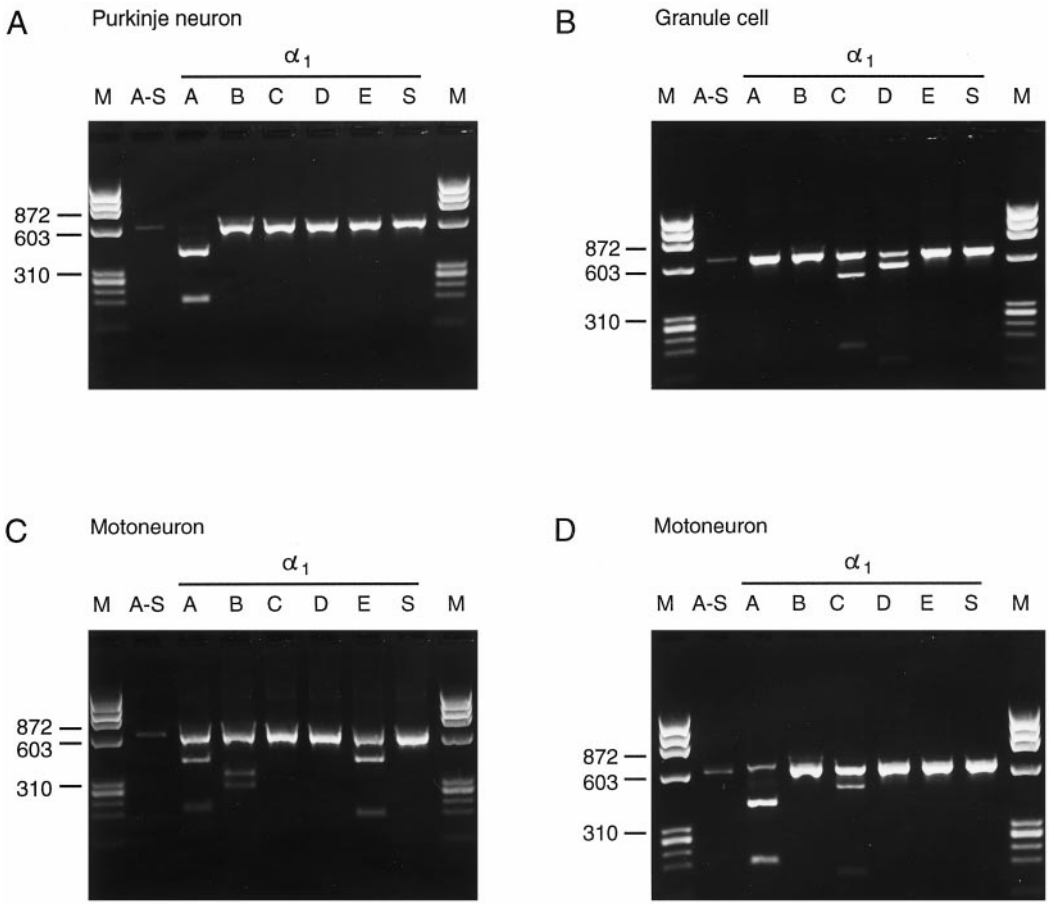

Figure 5. Single-cell RT-PCR analysis of Ca^{2+} channel α_1-subunit RNA expression in single neurons. Agarose gel electrophoresis of the cDNA amplified products from four single cells: (*A*) a cerebellar Purkinje neuron (Pn2), (*B*) a granule cell of the hippocampal dentate gyrus (Gc5), and (*C*, *D*) motoneurons from the facial nucleus (Mn24 and Mn20, respectively). Lanes marked *M* show the molecular weight marker ϕX174/*Hae*III. The lanes marked *A-S* show the band corresponding to the fragments obtained after the first PCR. Lanes marked *A, B, C, D, E,* and *S* show the fragments obtained after a second PCR reaction and restriction digest with the enzymes *Drd*I, *Bpm*I, *Hinc*II, *Afl*II, *Acc*I and *Cla*I, respectively.

accurately, was ~5% ($n = 5$). Similar effects were seen in two cells with nimodipine (10 μM). No difference was observed in the size of the effect of dihydropyridines when applied before (in three cells) or, as in Figure 6*B*, after (four cells) the other specific toxins, suggesting that it inhibited a component of current insensitive to the other toxins. These results suggest that in this preparation only a very small proportion of the current through Ca^{2+} channels is contributed by flow through L-type channels.

Effect of ω-Aga-IVA

ω-Aga-IVA inhibits P-type Ca^{2+} currents with a high affinity and Q-type currents with a lower affinity (Randall and Tsien, 1995). Despite the well documented effects on transmitter release at the axon terminals (Uchitel et al., 1992; Protti and Uchitel, 1993; Katz et al., 1996, 1997; Protti and Uchitel, 1997), in the cell bodies of facial motoneurons, ω-Aga-IVA had only very weak effects, if any. With a concentration of 100 nM ω-Aga-IVA or ω-Aga-TK, no block was observed in five cells (Fig. 7*A,B*), whereas in two others the current slowly decreased during toxin application to ~75-80% of the control value. In different cells, concentrations of ω-Aga-IVA up to 1 μM had effects similar to those with 100 nM, showing either a small decrease or no effect. In cells in which a small decrease in current was observed, the block could not be removed by repetitive depolarizations (10 pulses of 60 msec at 1 Hz) to +130 mV after washout of the toxin from the bath solution. This is in contrast to the reported effect on P-type channels for which the inhibition is normally relieved by strong depolarization [Mintz et al. (1992) and see below]. When compared with other brainstem motoneurons at similar postnatal ages that show a considerable block by ω-Aga-IVA (Umemiya and Berger, 1994), these effects of ω-Aga-IVA were surprising. To check that the toxin used was active, we performed control experiments in cerebellar Purkinje neurons, in which most of the current is contributed by P-type channels (Llinás et al., 1992; Mintz et al., 1992), at an age (P4–P8) when the cells have few dendritic processes and can be well voltage-clamped. In three Purkinje neurons, ω-Aga-IVA (100 nM) blocked the Ca^{2+} current by ~80% (Fig. 7*C,D*). The block was not reversed on washout of the toxin from the bath, but it was completely removed by three trains of depolarizations to +130 mV (Fig. 7*C,D*) (also see Mintz et al., 1992).

Effects of ω-CTx-MVIIC

As a further test to substantiate the contribution of N- and P/Q-type channels, we also tested the toxin ω-CTx-MVIIC (Hillyard et al., 1992). This toxin inhibits currents through N- and P/Q-type Ca^{2+} channels, with more rapid effects on N-type than on P- or Q-type channels (Randall and Tsien, 1995; McDonough et al., 1996). When added alone, ω-CTx-MVIIC clearly had a rapid inhibitory effect that resembled that of ω-CTx-GVIA in

Table 2. Ca^{2+} channel α_1-subunit mRNA detected in single neurons

			Subunit					
Cell	Nucleus	Age	α_{1A}	α_{1B}	α_{1C}	α_{1D}	α_{1E}	α_{1S}
Pn 1	−	P18	+	−	−	−	−	−
Pn 2	+	P18	+	−	−	−	−	−
Pn 3	+	P18	+	−	−	−	−	−
Pn 4	+	P18	+	−	−	−	−	−
Gc 1	+	P6	+	+	−	+	−	−
Gc 5	+	P6	−	−	+	+	−	−
Gc 6	+	P6	+	+	−	+	+	−
Mn 2	−	P4	+	−	−	+	+	−
Mn 3	−	P4	−	+	−	−	−	−
Mn 4	−	P4	+	+	−	−	+	−
Mn 6	−	P4	−	+	−	−	+	−
Mn 8	−	P4	+	−	−	−	−	−
Mn 9	+	P4	+	+	−	−	+	−
Mn 10	+	P4	−	+	−	−	−	−
Mn 11	−	P4	+	−	−	−	+	−
Mn 13	+	P2	+	+	−	−	−	−
Mn 14	−	P2	+	+	−	+	+	−
Mn 15	−	P2	+	+	+	−	−	−
Mn 16	−	P3	+	+	−	−	+	−
Mn 18	−	P3	+	−	−	+	+	−
Mn 20	−	P4	+	−	+	−	−	−
Mn 21	+	P4	+	−	+	−	+	−
Mn 23	−	P1	+	+	−	−	+	−
Mn 24	+	P1	+	+	−	−	+	−
Mn 25	−	P2	+	+	−	+	−	−
Mn 26	−	P2	+	−	+	−	+	−
Mn 30	+	P4	+	−	−	−	−	+
Mn 31	+	P2	+	−	−	−	−	+
Mn 32	−	P2	+	+	−	−	+	−

Pn, Purkinje neuron; Gc, hippocampal dentate gyrus granule cell; Mn, facial motoneuron. The column labeled nucleus indicates whether the nucleus was harvested together with the cytoplasm.

time course and extent (Fig. 8*A*), with no slow component of inhibition. In four cells, a concentration of 1 μM ω-CTx-MVIIC reduced the current by 22 ± 4%, whereas in one other cell the current was unaffected. In contrast, in three cells pretreated with ω-CTx-GVIA (1 μM) for some minutes, which caused a block like that described above (Fig. 6*A*), ω-CTx-MVIIC (1 μM) had no additional inhibitory effect on the Ca^{2+} channel current (Fig. 8*B*).

The current that remained at −10 mV after inhibition by ω-CTx-MVIIC (Fig. 8*A*) or ω-CTx-GVIA (Fig. 6*A*) was similar in time course to that before toxin treatment. In the cells that were treated with ω-CTx-MVIIC, the current had decayed to 88.0 ± 0.6% of the peak value at the end of the 50 msec test pulse before toxin treatment and 84.3 ± 0.7% after toxin treatment. Thus, the toxin-resistant component of current at −10 mV does not resemble T-type current (Huguenard, 1996) or the R-type described in cerebellar granule neurons (Randall and Tsien, 1995), both of which inactivate more rapidly. We therefore designate this current R_{slow}. Measurement of the *I–V* relation after the application of ω-CTx-MVIIC or ω-CTx-GVIA indicated that both LVA and HVA current components were present after toxin treatment and that the peak of the *I–V* relation remained at −10 mV (data not shown).

Comparison of pharmacological and RT-PCR data

None of the cells studied showed a clear, reversible response to ω-Aga-IVA, but the α_{1A}-subunit was detected in 86% of neurons (Table 2). In contrast, for the other α_1-subunits that can be pharmacologically differentiated, the proportion of cells that responded to the antagonist was higher than that in which the respective α_1-subunit was detected. Thus, 87% of neurons responded to either of the conotoxins, whereas α_{1B} was detected in 59%. Responses to dihydropyridines, albeit very small, were observed in 90% of cells, but α_{1C} or α_{1D} was detected in only 36%.

DISCUSSION

The main findings of this study on Ca^{2+} channels in facial motoneurons are as follows. (1) A major component of the Ca^{2+} current is carried by a channel R_{slow}, which is insensitive to inhibitory toxins and DHPs but unlike the R-type channel originally described in cerebellar granule neurons. N-, T-, and L-type components are also present. (2) The partially degenerate primers that were designed amplify all known HVA Ca^{2+} channel α_1-subunits and provide a powerful tool to identify the subunits present in a single cell. (3) With single-cell RT-PCR, highly heterogeneous patterns of Ca^{2+} channel α_1-subunit mRNA expression were detected in individual facial motoneurons. The dominant pattern was α_{1A} with α_{1B} and α_{1E}. However, α_{1C}, α_{1D}, and α_{1S} were detected in combination with the other subunits. In contrast, in cerebellar Purkinje neurons, only α_{1A} was detected. (4) Evidence with the toxins ω-Aga-IVA and ω-CTx-MVIIC indicated that P/Q-type Ca^{2+} channels are not present in the soma of facial motoneurons, whereas previous studies have shown that P-type channels dominate in the control of transmitter release at the nerve terminal. α_{1A}-subunit mRNA that is thought to code for P-type channels was detected in the majority of motoneurons.

Ca^{2+} current types identified in facial motoneurons

Nearly all neurons expressed LVA and HVA channels. Of the HVA current at −10 mV, ~30% was contributed by N-type Ca^{2+} channels, a proportion similar to that in rat hypoglossal motoneurons in slices (29%) (Umemiya and Berger, 1994), but less than that in a previous report on facial motoneurons (~50% with 50 μM) (Umemiya et al., 1993) and in reports on cultured embryonic rat and mouse spinal motoneurons (42-54%) (Mynlieff and Beam, 1994; Hivert et al., 1995; Viana et al., 1997). L-type channels contributed only a relatively minor component (~5%), as in hypoglossal motoneurons (6%) (Umemiya and Berger, 1994). The surprising result of this study was that the major component of the Ca^{2+} current was insensitive to specific inhibitors, including the inhibitor of P/Q-type channels, ω-Aga-IVA, and the inhibitor of N- and P/Q-type channels, ω-CTx-MVIIC, after inhibition of the N-type current. At the low extracellular Ba^{2+} concentration, all of the known channel types should have been blocked by the concentrations of toxins tested. The results with ω-CTx-MVIIC and ω-Aga-IVA, a toxin that had effects similar to those reported previously in cerebellar Purkinje neurons (Mintz et al., 1992), suggest that P/Q-type channels do not contribute significantly to the somatic/dendritic Ca^{2+} current in facial motoneurons. This finding contrasts with those on HVA Ca^{2+} channel currents in most motoneurons, even other brainstem motoneurons, studied to date that are inhibited by ω-Aga-IVA [hypoglossal motoneurons: 50% (Umemiya and Berger, 1994); embryonic rat spinal motoneurons: 10-30% (Hivert et al., 1995; Viana et al., 1997; Magnelli et al., 1998)] at concentrations

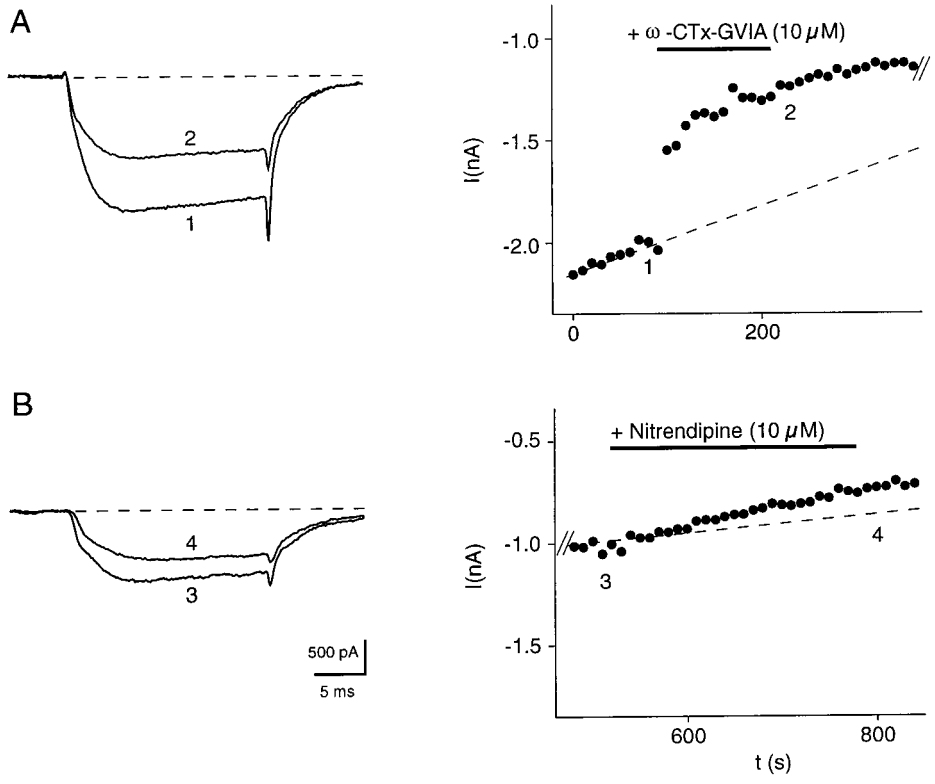

Figure 6. Inhibition of the Ca^{2+} channel current by ω-CTx-GVIA and nitrendipine. *A*, *Left*, Currents recorded during 20 msec potential steps from a V_h of −80 to −10 mV at the times indicated in the plot of peak current amplitude at −10 mV against time (*right*) illustrating the irreversible inhibition by ω-CTx-GVIA. *B*, *Left*, Currents recorded during 20 msec potential steps from a V_h of −80 mV to −10 mV before (*3*) and after (*4*) the addition of nitrendipine (10 μM). *Right*, Plot of peak current amplitude at −10 mV against time illustrating the inhibition by nitrendipine (10 μM). *B* is a continuation of the experiment in *A*.

that suggest that they are carried by P-type channels. However, recent studies on the latter preparation report that some (Viana et al., 1997) or as many as 60% of neurons (Magnelli et al., 1998) do not respond to ω-Aga-IVA.

R_{slow}, the current that was resistant to inhibition in facial motoneurons, displayed only little inactivation and thus resembles neither the antagonist-resistant R-type current in cerebellar granule neurons (Randall and Tsien, 1995) nor a residual LVA current. The latter was suggested for the current remaining after block of L-, N-, and P/Q-type channels in hypoglossal motoneurons (Umemiya and Berger, 1994). In contrast, the current remaining at potentials above −30 mV in facial motoneurons was clearly HVA. Interestingly, a slowly inactivating, antagonist-resistant current similar to that described here has also been observed recently and studied in detail in embryonic rat motoneurons (Magnelli et al., 1998). This current had biophysical properties, a divalent cation permeability, and a sensitivity to Ni^{2+} and Cd^{2+} more typical of HVA channels.

PCR analysis of Ca^{2+} channel α_1-subunit expression

In total RNA from rat brain, the detected pattern of HVA Ca^{2+} channel subunits reflected the region-specific expression of RNA shown previously by *in situ* hybridization (Tanaka et al., 1995; Ludwig et al., 1997). The pattern in other tissues is mainly that expected from previous studies or predicted from the known pharmacological properties of the Ca^{2+} channel currents. In single neurons we also observed a highly cell-specific pattern. Only α_{1A} was detected in cerebellar Purkinje neurons, known from the toxin sensitivity of their Ca^{2+} channel currents to mainly express P-type channels (Mintz et al., 1992). In contrast, in granule cells of the dentate gyrus and motoneurons of the facial nucleus, which like the majority of central neurons express multiple channel types, the pattern was more heterogeneous. The most frequently detected subunits in facial motoneurons were α_{1A}, α_{1B}, and α_{1E}, in agreement with data from *in situ* hybridization for this nucleus (Tanaka et al., 1995).

Ca^{2+} channel α_1-subunit expression and localization in motoneurons

Compared with the pharmacological data, the biggest surprise was the large fraction of facial motoneurons in which mRNA for α_{1A} was detected, despite the lack of clear pharmacological evidence for functional P/Q-type channels. This could be explained by the absence of functional P/Q-type channels in the soma and proximal dendrites, with specific segregation of this channel type to the neuromuscular junction, where it has been shown to be involved in the release of transmitter. This interpretation is supported by a report on spinal cord motoneurons (Westenbroek et al., 1998) showing by immunocytochemistry that the α_{1A}-subunit is localized presynaptically at the neuromuscular junction, but that the staining on the soma and dendrites is more consistent with a presynaptic localization. Of the other subunits, α_{1C}, α_{1D}, and α_{1E} were present in the soma, and α_{1B} was present in the soma and dendrites and occasionally at the NMJ. Other immunocytochemical and pharmacological studies confirm the presence and important role of α_{1A} at the NMJ. Thus, an antibody specific for the Ca^{2+} channel α_{1A}-subunit labels the NMJ in the diaphragm preparation of adult rats (Ousley and Froehner, 1994). Furthermore, in studies at the adult mammalian neuromuscular junction, mostly at endplates that are innervated by the facial nerve, transmitter release and presynaptic currents (both Ca^{2+} and Ca^{2+}-dependent K^+ currents) were strongly inhibited by ω-Aga-IVA but unaffected by ω-CTx-GVIA and nitrendipine, suggesting that Ca^{2+} entry mainly occurs through P-type Ca^{2+} channels (Uchitel et al., 1992; Protti and Uchitel, 1993; Katz et al., 1996, 1997; Protti and Uchitel, 1997). In neonatal rats (P0–P9), transmitter release from facial motoneuron nerve terminals is also strongly inhibited by ω-Aga-IVA (M. D. Rosato Siri and

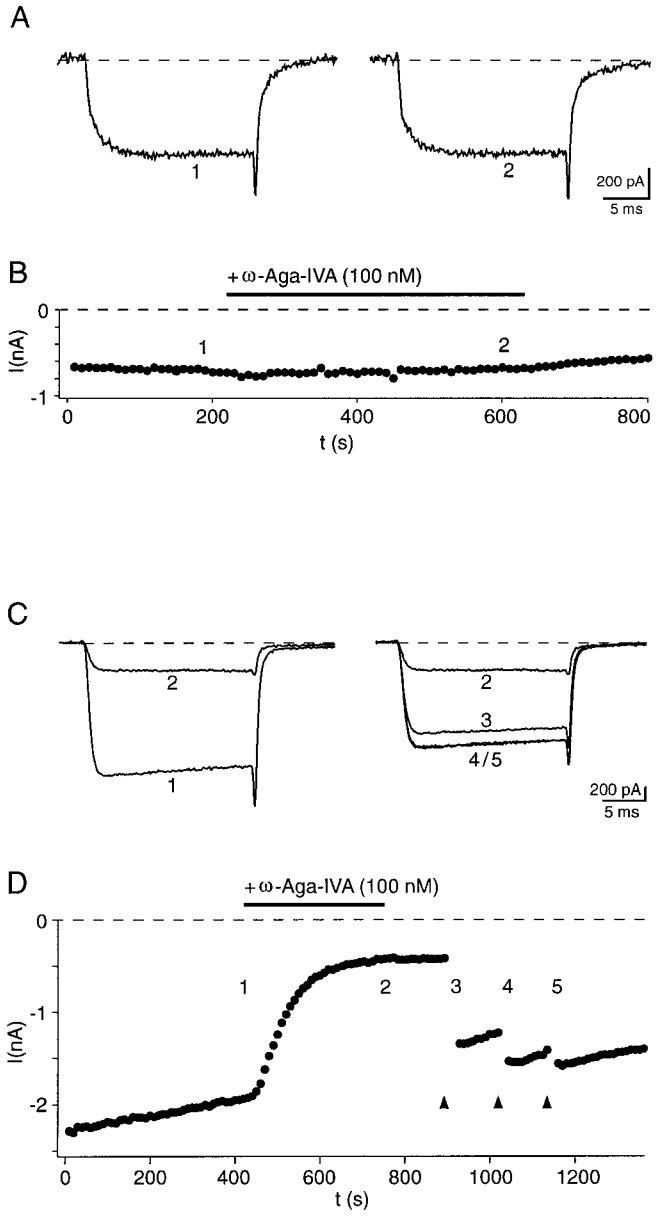

Figure 7. Lack of effect of ω-Aga-IVA on Ca^{2+} channel currents in motoneurons but clear effects in cerebellar Purkinje neurons. *A, B*, Effects of ω-Aga-IVA in motoneurons. *A*, Currents recorded at −10 mV at the times indicated in *B*, before (*1*) and during (*2*) the application of ω-Aga-IVA to the bath solution. *B*, Plot of the peak current against time showing that 100 nM ω-Aga-IVA had no effect on the Ca^{2+} channel current. *C, D*, Inhibition of Ca^{2+} channel currents in cerebellar Purkinje neurons by ω-Aga-IVA. *C*, Ba^{2+} currents recorded during 20 msec impulses to −10 mV from a holding potential of −70 mV in a Purkinje neuron in a cerebellar slice from a 4-d-old rat. The currents were recorded at the times indicated in *D*, in the control (*1*), after inhibition by 100 nM ω-Aga-IVA (*2*), after washout of toxin from the bath and one train of 10 pulses of 60 msec duration to +130 mV (*3*), and after a second and third train of depolarizations (*4* and *5*, respectively). *D*, Plot of peak current at −10 mV against time showing the time course of current block by ω-Aga-IVA and its removal by strong depolarizations. The trains of depolarizations were applied at the times indicated by the *filled triangles*.

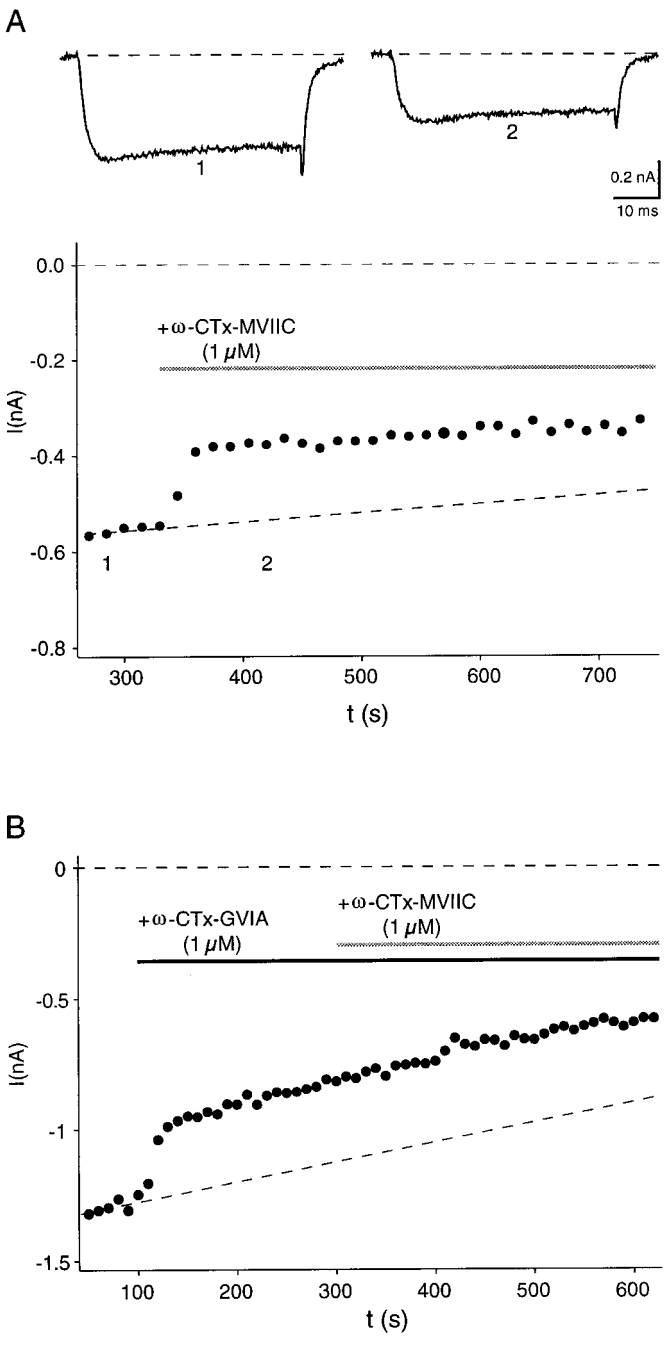

Figure 8. Block of the Ca^{2+} channel current in motoneurons by ω-CTx-MVIIC. *A*, Inhibition of the Ca^{2+} channel current at −10 mV by 1 μM ω-CTx-MVIIC. The current records (*top part*) were measured at the times indicated in plot of current amplitude at −10 mV against time during the experiment (*bottom part*). The toxin was added to the bath in the absence of perfusion. *B*, Lack of effect of ω-CTx-MVIIC when applied after ω-CTx-GVIA. In this experiment, ω-CTx-GVIA (1 μM) was added to the bath. After a stable level of inhibition was reached, ω-CTx-MVIIC (1 μM) was also added. Peak currents were recorded at −10 mV during steps from −80 mV.

O. D. Uchitel, unpublished observations). Therefore, it seems likely that motoneurons express different Ca^{2+} channel types at the axon terminal than at the soma (Fig. 9).

An alternative explanation, which would also account for the antagonist-insensitive current in the soma, is the expression of different forms of channels containing the α_{1A}-subunit at different subcellular sites: a toxin-resistant form of channel in the soma and a toxin-sensitive form at the axon terminal. The auxiliary subunits of the Ca^{2+} channel, especially the β-subunit, can strongly influence both the expression and functional properties,

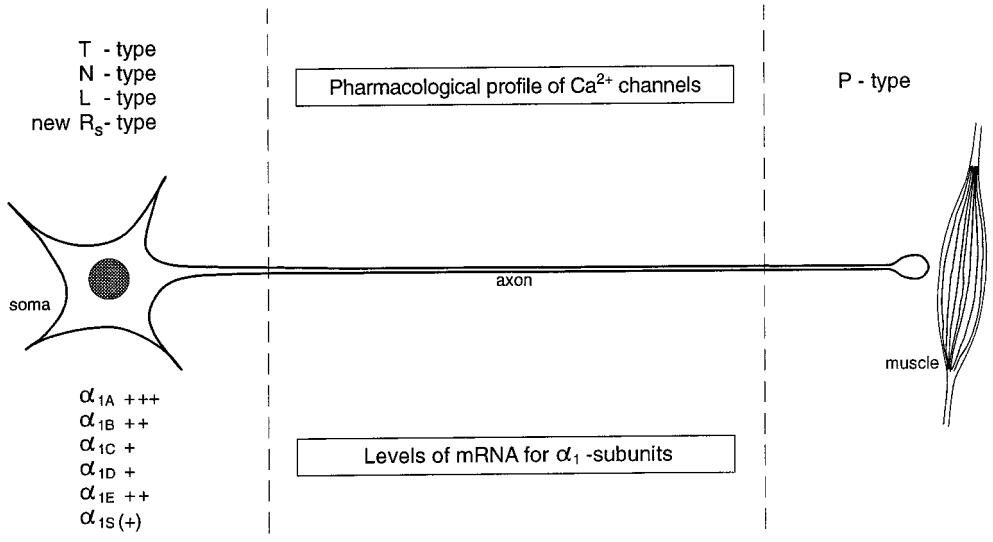

Figure 9. Scheme of a facial motoneuron summarizing the proposed subcellular distribution of Ca^{2+} channel types from functional studies and the α_1-subunit mRNA expression pattern from RT-PCR. + indicates the proportion of cells in which the subunit was detected.

including the toxin sensitivity, of the α_1-subunits (Moreno et al., 1997; Tareilus et al., 1997). Thus, in the absence of the appropriate β-subunit or expression of a different β-subunit in a subcellular region, α-subunits may not be expressed or may have very different properties, respectively. Likewise, antagonist-insensitive channels could result from the α_{1E}-subunit, thought to compose the toxin resistant channels in cerebellar granule neurons (Randall and Tsien, 1995), with slowed inactivation determined by the β-subunit (Parent et al., 1997). mRNA for α_{1E} was detected in many although not all neurons. From our RT-PCR data, we cannot identify the α_1-subunit type that corresponds to R_{slow}. The experiments provided no evidence with the primers used for a novel α_1-subunit.

The α_{1B}-subunit was not detected in all neurons, although most responded to ω-CTx-GVIA or ω-CTx-MVIIC. This may just result from a low abundance of the mRNA at the time of harvesting the cytoplasm in some cells and not indicate that functional channels are absent. A similar conclusion was reached in another study using single-cell RT-PCR in neostriatal interneurons (Yan and Surmeier, 1996). There, a highly heterogeneous pattern of mRNA expression was detected in individual cells, but the pharmacological profile reflected the functional expression of all of the channel types in each neuron. The detection in facial motoneurons of α_{1C} and α_{1D} mRNAs in only a small proportion of cells most probably reflects their low abundance and their minor contribution to the whole-cell current.

In conclusion, T-, N-, and L-type Ca^{2+} channels together with a major toxin-resistant component R_{slow}, which does not resemble the R-type in other neurons, are present in the soma of neonatal facial motoneurons. Although no P/Q-type current was measured in the soma, mRNA for this subunit was dominant. This result, together with the results of studies of Ca^{2+} channels involved in transmitter release at the nerve terminal, suggests that there are strong subcellular regional differences in Ca^{2+} channel expression in facial motoneurons. Remarkably, the Ca^{2+} channel pattern found in motoneurons in the facial nucleus is distinctly different from that found in other brainstem motoneurons.

REFERENCES

Bargas J, Howe A, Eberwine J, Cao Y, Surmeier DJ (1994) Cellular and molecular characterization of Ca^{2+} currents in acutely isolated, adult rat neostriatal neurons. J Neurosci 14:6667-6686.

Catterall WA (1995) Structure and function of voltage-gated ion channels. Annu Rev Biochem 64:493-531.

Chin H, Krall M, Kim H-L, Kozak CA, Mock B (1992) The gene for the α_1 subunit of the skeletal muscle dihydropyridine-sensitive calcium channel (Cchl1a3) maps to mouse chromosome 1. Genomics 14:1089-1091.

Dunlap K, Luebke JI, Turner TJ (1995) Exocytotic Ca^{2+} channels in mammalian central neurons. Trends Neurosci 18:89-98.

Edwards FA, Konnerth A, Sakmann B, Takahashi T (1989) A thin slice preparation for patch clamp recordings from neurones of the mammalian central nervous system. Pflügers Arch 414:600-612.

Eliot LS, Johnston D (1994) Multiple components of calcium current in acutely dissociated dentate gyrus granule neurons. J Neurophysiol 72:762-777.

Hillyard DR, Monje VD, Mintz IM, Bean BP, Nadasdi L, Ramachandran J, Miljanich G, Azimi-Zoonooz A, McIntosh JM, Cruz LJ, Imperial JS, Olivera BM (1992) A new Conus peptide ligand for mammalian presynaptic Ca^{2+} channels. Neuron 9:69-77.

Hivert B, Bouhanna S, Diochot S, Camu W, Dayanithi G, Henderson CE, Valmier J (1995) Embryonic rat motoneurons express a functional P-type voltage-dependent calcium channel. Int J Dev Neurosci 13:429-436.

Hofmann F, Biel M, Flockerzi V (1994) Molecular basis for Ca^{2+} channel diversity. Annu Rev Neurosci 17:399-418.

Huguenard JR (1996) Low-threshold calcium currents in central nervous system neurons. Annu Rev Physiol 58:329-348.

Katz E, Ferro PA, Weisz G, Uchitel OD (1996) Calcium channels involved in synaptic transmission at the mature and regenerating mouse neuromuscular junction. J Physiol (Lond) 497:687-697.

Katz E, Protti DA, Ferro PA, Siri MDR, Uchitel OD (1997) Effects of Ca^{2+} channel blocker neurotoxins on transmitter release and presynaptic currents at the mouse neuromuscular junction. Br J Pharmacol 121:1531-1540.

Lambolez B, Audinat E, Bochet P, Crépel F, Rossier J (1992) AMPA receptor subunits expressed by single Purkinje cells. Neuron 9:247-258.

Llinás R, Sugimori M, Hillman DE, Cherskey B (1992) Distribution and functional significance of the P-type, voltage-dependent Ca^{2+} channels in the mammalian central nervous system. Trends Neurosci 15:351-355.

Llinás R, Sugimori M, Cherksey BD, Smith RG, Delbono O, Stefani E, Appel S (1993) IgG from amyotrophic lateral sclerosis patients increases current through P-type calcium channels in mammalian cerebellar Purkinje cells and in isolated channel protein in lipid bilayer. Proc Natl Acad Sci USA 90:11743-11747.

Ludwig A, Flockerzi V, Hofmann F (1997) Regional expression and cellular localization of the α_1 and β subunit of high voltage-activated calcium channels in rat brain. J Neurosci 17:1339-1349.

Magnelli V, Baldelli P, Carbone E (1998) Antagonists-resistant calcium currents in rat embryo motoneurons. Eur J Neurosci 10:1810-1825.

McDonough SI, Swartz KJ, Mintz IM, Boland LM, Bean BP (1996)

Inhibition of calcium channels in rat central and peripheral neurons by omega-conotoxin MVIIC. J Neurosci 16:2612-2623.

Mintz IM, Adams ME, Bean BP (1992) P-type calcium channels in rat central and peripheral neurons. Neuron 9:85-95.

Mogul DJ, Fox AP (1991) Evidence for multiple types of Ca^{2+} channels in acutely isolated hippocampal CA3 neurons of the guinea pig. J Physiol (Lond) 433:259-281.

Moreno H, Rudy B, Llinás R (1997) β subunits influence the biophysical and pharmacological differences between P- and Q-type calcium currents expressed in a mammalian cell line. Proc Natl Acad Sci USA 94:14042-14047.

Mosier DR, Baldelli P, Delbono O, Smith RG, Alexianu ME, Appel SH, Stefani E (1995) Amyotrophic lateral sclerosis immunoglobulins increase Ca^{2+} currents in a motoneuron cell line. Ann Neurol 37:102-109.

Mynlieff M, Beam KG (1992) Characterization of voltage-dependent calcium currents in mouse motoneurons. J Neurophysiol 68:85-92.

Mynlieff M, Beam KG (1994) Adenosine acting at an A1 receptor decreases N-type calcium current in mouse motoneurons. J Neurosci 14:3628-3634.

Olivera BM, McIntosh JM, Cruz LJ, Luque FA, Gray WR (1984) Purification and sequence of a presynaptic peptide toxin from *Conus geographus* venom. Biochemistry 23:5087-5090.

Olivera BM, Miljanich GP, Ramachandran J, Adams ME (1994) Calcium channel diversity and neurotransmitter release: the omega-conotoxins and omega-agatoxins. Annu Rev Biochem 63:823-867.

Ousley AH, Froehner SC (1994) An anti-peptide antibody specific for the class A calcium channel α_1 subunit labels mammalian neuromuscular junction. Proc Natl Acad Sci USA 91:12263-12267.

Parent L, Schneider T, Moore CP, Talwar D (1997) Subunit regulation of the human brain α_{1E} calcium channel. J Membr Biol 160:127-140.

Perez-Reyes E, Cribbs LL, Daud A, Lacerda AE, Barclay J, Williamson MP, Fox M, Rees M, Lee J-H (1998) Molecular characterization of a neuronal low-voltage-activated T-type calcium channel. Nature 391:898-900.

Plant T, Schirra C, Garaschuk O, Rossier J, Konnerth A (1997) Molecular determinants of NMDA receptor function in GABAergic neurones of rat forebrain. J Physiol (Lond) 499:47-63.

Protti DA, Uchitel OD (1993) Transmitter release and presynaptic Ca^{2+} currents blocked by the spider toxin omega-Aga-IVA. NeuroReport 5:333-336.

Protti DA, Uchitel OD (1997) P/Q-type calcium channels activate neighboring calcium-dependent potassium channels in mouse motor nerve terminals. Pflügers Arch 434:406-412.

Randall A, Tsien RW (1995) Pharmacological dissection of multiple types of Ca^{2+} channel currents in rat cerebellar granule neurons. J Neurosci 15:2995-3012.

Regan LJ, Sah DW, Bean BP (1991) Ca^{2+} channels in rat central and peripheral neurons: high threshold current resistant to dihydropyridine blockers and ω-conotoxin. Neuron 6:269-280.

Stocker JW, Nadasdi L, Aldrich RW, Tsien RW (1997) Preferential interaction of omega-conotoxins with inactivated N-type Ca^{2+} channels. J Neurosci 17:3002-3013.

Stuart GJ, Dodt H-U, Sakmann B (1993) Patch-clamp recordings from the soma and dendrites of neurons in brain slices using infrared video microscopy. Pflügers Arch 423:511-518.

Tanaka O, Sakagami H, Kondo H (1995) Localization of mRNAs of voltage-dependent Ca^{2+}-channels: four subtypes of α1- and β-subunits in developing and mature rat brain. Mol Brain Res 30:1-16.

Tareilus E, Roux M, Qin N, Olcese R, Zhou JM, Stefani E, Birnbaumer L (1997) A *Xenopus* oocyte β subunit: evidence for a role in the assembly/expression of voltage-gated calcium channels that is separate from its role as a regulatory subunit. Proc Natl Acad Sci USA 94:1703-1708.

Uchitel OD, Appel SH, Crawford F, Sczcupak L (1988) Immunoglobulins from amyotrophic lateral sclerosis patients enhance spontaneous transmitter release from motor-nerve terminals. Proc Natl Acad Sci USA 85:7371-7374.

Uchitel OD, Protti DA, Sanchez V, Cherksey BD, Sugimori M, Llinás R (1992) P-type voltage-dependent calcium channel mediates presynaptic calcium influx and transmitter release in mammalian synapses. Proc Natl Acad Sci USA 89:3330-3333.

Umemiya M, Berger AJ (1994) Properties and function of low- and high-voltage-activated Ca^{2+} channels in hypoglossal motoneurons. J Neurosci 14:5652-5660.

Umemiya M, Berger AJ (1995) Single-channel properties of four calcium channel types in rat motoneurons. J Neurosci 15:2218-2224.

Umemiya M, Araki I, Kuno M (1993) Electrophysiological properties of axotomized facial motoneurones that are destined to die in neonatal rats. J Physiol (Lond) 462:661-678.

Viana F, Bayliss D, Berger AJ (1993) Calcium conductances and their role in the firing behavior of neonatal rat hypoglossal motoneurons. J Neurophysiol 69:2137-2149.

Viana F, Van den Bosch L, Missiaen L, Vandenberghe W, Droogmans G, Nilius B, Robberecht W (1997) Mibefradil (Ro 40-5967) blocks multiple types of voltage-gated calcium channels in cultured rat spinal motoneurones. Cell Calcium 22:299-311.

Westenbroek RE, Hoskins L, Catterall WA (1998) Localization of Ca^{2+} channel subtypes on rat spinal motoneurons, interneurons, and nerve terminals. J Neurosci 18:6319–6330.

Wheeler DB, Randall A, Sather WA, Tsien RW (1995) Neuronal calcium channels encoded by the α_{1A} subunit and their contribution to excitatory synaptic transmission in the CNS. In: Gene expression in the central nervous system (Yu ACH, Eng LF, McMahan KJ, Schulman H, Shooter EM, Stadlin A, eds), pp 65-76. Amsterdam: Elsevier.

Yan Z, Surmeier DJ (1996) Muscarinic (m2/m4) receptors reduce N- and P-type Ca^{2+} currents in rat neostriatal cholinergic interneurons through a fast, membrane-delimited, G-protein pathway. J Neurosci 16:2592-2604.